ASPECTS OF FRACTURE PROCESSES IN PAPER

Lauri Salminen

Laboratory of Physics
Helsinki University of Technology
Espoo, Finland

Dissertation for the degree of Doctor of Science in Technology to be presented with due permission of the Department of Engineering Physics and Mathematics, Helsinki University of Technology for public examination and debate in Auditorium E at Helsinki University of Technology (Espoo, Finland) on the 5th of June, 2003, at 12 o'clock noon.

Dissertations of Laboratory of Physics, Helsinki University of Technology
ISSN 1455-1802

Dissertation 122 (2003):
Lauri Salminen: Aspects of Fracture Processes in Paper
ISBN 951-22-6555-9 (print)
ISBN 951-22-6556-7 (electronic)

OTAMEDIA OY
ESPOO 2003

Abstract

The strength properties and fracture processes are studied in paper. This thesis deals with the fundamental structure and physical phenomenon of fracture. The methods employed are Monte Carlo simulations with a finite element model and experiments in fractography and acoustic emission.

It is still unclear how the mechanical properties of paper, particularly strength depend on the disordered geometry of the fiber network. The shrinkage during manufacturing process induces internal stresses, which are crucial to macroscopic properties. The limiting strength in paper depends on crack pinning effects and obeys extremal statistics. The local stress variations introduce crack pinning and affect the fracture line topography.

In the thesis geometrical effects of fiber network shrinkage are simulated and observed to follow a simple analytic expression. The shrinkage of fiber segments agrees qualitatively with microscopic measurements in literature. Extensive tensile strength distributions are obtained and compared with theoretical strength models. The strength of paper is found to be close to the Weibull and Duxbury distributions. Crack localization in tensile mode I loading is studied with initially notched strips. The resulting pinning probability agree with simple simulations and demonstrates that paper tolerates short order of fiber length notches. The fractal nature of paper crack line is analyzed in large samples. The geometry in fast crack propagation is found to be self-affine with a roughness exponent close to 0.6. The value is not in agreement with any fracture models. In addition systematic deviations from pure power law dependence is observed in the length-scale 5 – 20 mm.

Acoustic emission spectroscopy is employed to study paper fracture in tensile and peel tests. By acoustic emission the energy released in micro fracturing is measured. The energy statistics are observed to obey power law analogously to Gutenberg-Richter's law for eartchquakes. In the tensile test the exponent characterizing the energy distribution is 1.2 and in the peel test 2.0. In the tensile tests the inter-arrival time between events obey a power law (Omori's law) with an exponent close to 1.0. In the peel tests deviations from Omori's power law are found. These observations suggest that the two often simultaneously witnessed power laws do no have a common origin. The acoustic emission results give new insight to fracture processes in the presence of disorder.

Preface

This thesis has been prepared in the Laboratory of Physics at the Helsinki University of Technology during the years 1997-2003.

I wish to express my gratitude to my advisors Docent Mikko Alava and Docent Kaarlo Niskanen for giving me the opportunity to participate in their enthusiastic scientific research. Their guidance in my studies has been invaluable for over 10 years.

I would also like to thank Academy Professor Risto Nieminen and Professor Pekka Hautojärvi for their encouragement and for providing excellent working facilities. I am grateful to all the coauthors and colleagues, especially Jari Rosti and Joonas Pulakka. I express my sincerest appreciation to the people in the Laboratory of Physics.

Finally, my heartfelt thanks belong to my sister and parents.

Ridasjärvi, May 2003

Lauri Salminen

Contents

List of publications

This thesis consists of an overview and the following publications:

I. M. Korteoja, L.I. Salminen, K.J. Niskanen, and M.J. Alava, "Strength Distribution in Paper", Material Science and Engineering A240, 173 – 180 (1998).

II. L.I. Salminen, M.J. Alava, S. Heyden, P-J. Gustafsson and K.J. Niskanen, "Simulation of Network Shrinkage", Nordic Pulp and Paper Research Journal Vol 17, No 2/2002, 105 – 110.

III. J. Rosti, L.I. Salminen, E.T. Seppälä, M.J. Alava, and K.J. Niskanen, "Pinning of Cracks in Two-dimensional Disordered Media", European Physical Journal B19, 259 – 263 (2001).

IV. L.I. Salminen, M.J. Alava, and K.J Niskanen "Analysis of long crack lines in paper webs", European Physical Journal B32, 369 – 374 (2003).

V. L.I. Salminen, A.I. Tolvanen, and M.J. Alava, "Acoustic Emission from paper fracture", Physical Review Letters 89, 185503 (2002).

VI. L.I. Salminen, J.M. Pulakka, M.J. Alava, and K.J. Niskanen "Crackling noise in paper peeling", (submitted).

The roman numerals are used in this overview when referring to the Publications.

The author's contribution

The author has had an active role in all stages of the research reported in Publications II - VI. The author has performed the experiments in paper I and IV and the simulations in II. He has designed the apparatuses in paper VI and the experiments in papers III - VI. The measurement results in papers II, IV, V,VI have been analyzed by him. The Publications were produced in collaboration, the disputant having significant responsibility for writing Publications IV and VI.

Chapter 1

Introduction

Strength is an essential property describing the limiting mechanical load. Fracture is a phenomenon related to the loss of strength. This thesis approaches mainly experimentally the interdependence of various processes in paper fracture [1]. The strength of homogeneous materials is well-treated by continuum mechanics [2] and thus research is focusing on dynamics [3] and effects of disorder [4–7]. Paper is an industrial product in which the stochastic structure affects its strength and failure [8, 9].

Quantitative descriptions of temporal and spatial behavior in paper fracture and their impact in practice are still inadequate. The majority of the current knowledge of paper failure phenomena is based on qualitative microscopic observations. It is widely accepted - although also the opposite can be argued for rationally, too [10] - that in paper its disordered structure is significantly related to mechanical properties in tension [1, 8].

The objective of this thesis is to study paper fracture by novel methods and thus provide data to test microscopic fracture models. The geometrical characteristics, tensile strength, and dynamics of fracture process are studied in the statistical sense. The importance of pulping and paper making research must be admitted, although here they are excluded.

This thesis provides information concerning the variation of paper strength. The experimental tensile strength distribution agrees with Weibull and Duxbury distributions. The shrinkage in a fiber network, which has an influence on the fracture process, is studied by simulation. The effects of network structure and fiber properties on sheet shrinkage are assorted quantitatively. Also, the

geometry and localization of the fracture line are explored. The fracture line in paper is shown to be self-affine. In addition it is shown that paper tolerates small flaws.

An acoustic emission technique is adapted for paper fracture research. New characteristics, similar to those of earthquakes, in paper failure are demonstrated. The energies of elementary fracture events were found to be described by a power-law probability distribution similar to the Gutenberg-Richter-law [11] for earthquakes. Also the waiting times between the acoustic events were shown to follow a power-law distribution. This Omori's power-law [12] has a universal exponent. Two principal test geometries were employed, giving distinct energy exponents and essentially different waiting time distributions.

1.1 Prologue to Paper

The man credited for inventing paper is the Chinese Ts'ai Lun circa 100 AD. Today industrial paper manufacturing is a substantial business.

Microscopically the basic structure of paper is a stochastic network of wood fibers [9] (Figure 1.1). Hydrogen bonds account for the adhesion between fibers. The structure of the network is layered and almost two-dimensional. Paper height is typically 10 – 20 fiber heights, i.e. 100 μm or about one tenth of a fiber length. Representative areal mass i.e. basis weight of e.g. newsprint paper is 50 g/m^2. The characteristic cloudiness is an implication of inhomogeneous basis weight distribution, typical variation is 10 % of basis weight. One A4 sheet contains of the order of 10 million fibers. Besides the fibers, paper contains also fines and fillers.

Usually the cellulose fibers in paper originate from wood, non-wood fibers have importance locally and in specialty papers. Length is the most important characteristics of paper making fibers. The typical length is 0.8 – 1.2 mm for hardwoods and 3 – 8 mm for softwoods. Fiber widths range between 15 and 50 μm. The internal structure of fibers is layered, and the layers that dominate the mechanical behavior consist of fibrils at a constant angle. The fibrils are small bundles of cellulose fibers. In paper the elementary fastening links are presumably hydrogen bonds. The degree of bonding, i.e. the relative bonded area has crucial effects on several properties of paper. The relative bonded area can be controlled by e.g. pulp beating and wet pressing during the manufacturing.

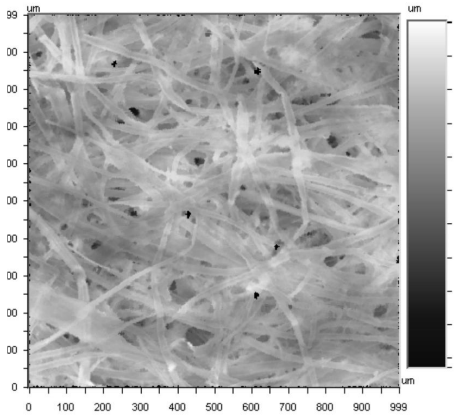

(a) Topography of paper by optical interferometry, dark accounts for areas of greater depth. The side length of the image is 1 mm. Courtesy of VTT.

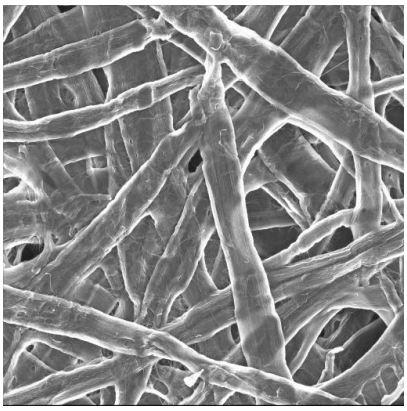

(b) An ESEM image of paper with a side length of about 360 μm. The difference in smoothness between the interferometry and ESEM images is due to the wavelength of light (≈ 0.7 μm). Courtesy of KCL.

Figure 1.1: The fibrous paper structure.

If external stress on paper is increased, at some point, some element of the fiber network is bound to break. The intrinsic paper fracture concepts are fiber-to-fiber bond breakage, fiber breakage, and a systematic combination of bond ruptures as fiber pull-out. The fibers are irregular, their surfaces are curved, and mismatches occur in bonding between two fibers. Together with bond periphery edge effects this leads to an oblique stress field. In thin sheets fracture is dominated by bond failures. In thicker sheets both bond and fiber failures appear simultaneously[8]. Most of the fiber failures are experimentally observed to be partial [13]. Bond openings which create new surfaces can be detected by an increased light scattering coefficient [14].

The pulping process, the method of wood disintegration into fibers, can be mechanical or chemical. The former is more economical, but results in some less desirable fiber properties than the chemical processing. After the defibering, the pulp is manipulated by e.g. bleaching and refining. During pulping, varying amounts of fine material is produced. The fines cover most of the fiber surfaces, and through their large specific area the fines improve bonding between fibers. A multitude of fillers like $CaCO_3$, and additives like starch, are used to trim the

manufacturing and to improve the end product properties.

Commercial paper is manufactured in a continuous manner in paper machines. From a 1 % pulp-water suspension in the headbox, the fibers are distributed on a wire screen. In the wire section over 50 per cent of the water is removed, and consolidated web is formed. Next the web is dewatered by wet pressing, and at the end of the drying section of the paper machine its solids content reaches 90 %. The velocity of the web is up to 20 m/s and a typical width of modern paper machine is 10 m.

The machine-made paper has a strong directional preference. This anisotropy is due to uneven fiber orientation and drying conditions. The velocity difference between the headbox jet and the wire results in more fibers being parallel to the machine direction (MD). During drying the paper web is under tension produced by the differential nip velocities. In the cross direction (CD) stress in lower. In the machine direction paper is more brittle and has larger elastic modulus and strength. In MD the strain at break is close to 1 % and in CD the maximum strain is up to 5 %. The behavior is more plastic and fracture is more ductile.

1.2 Mechanical Behavior

The strength - maximal load - is a straightforward mechanical property. Usually the mechanical properties of paper are measured by a tensile test, which is an implementation of the strain controlled mode I loading. In the case of paper the load-elongation behavior looks plain (Figure 1.2a), but includes quite a few phenomena, and rationalizations for many of these are missing.

The stress-strain curve is usually characterized by three ratings: elastic modulus, strain at break and tensile strength. Elastic modulus E_0 is defined as the initial slope of the load-elongation curve, and tensile strength σ_{max} is determined by the maximum stress value. The strain corresponding to maximal stress is defined as the strain at break ϵ_{max}. The stress-strain curve of cyclic loading (Figure 1.2b) illustrates the fact that paper exhibits both ideally elastic properties and plastic characteristics [1, 9]. The elastic modulus remains almost the same during the loading (Figure 1.3a). Thus the plastic strain ϵ_{pl} can be approximated by the equation $\epsilon_{pl} = \epsilon - \sigma/E_0$. In addition, paper is viscous and its mechanical properties depend somewhat on the rate of elongation $\dot{\epsilon}$. The general trend is that the higher the speed of elongation, the higher is the elastic modulus and the lower the strain at break. Also the ambient affects the strength, and

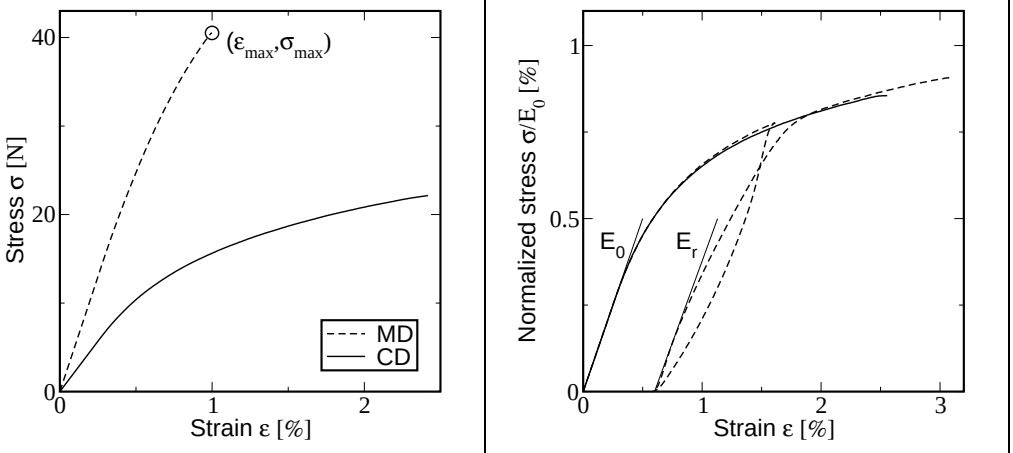

(a) Stress-strain curve in the machine (MD) and cross machine directions (CD).

(b) A cyclic stress-strain curve demonstrating the initial elastic modulus E_0 and the reloading modulus E_r.

Figure 1.2: Examples of stress-strain curves of paper.

humidity has a considerably large influence because water contents increases the plasticity in paper. Compared to humidity, the influences of temperature and strain rate are small. By standardization the effects of experimental conditions can be minimized, and test results are useful for paper characterization [15, 16].

The stress-strain behavior of paper has quite a fixed form compared to the stress-strain curves of its constituents. So changes in the furnish properties are not transferred entirely to paper properties. Despite of the significant diversification in the constituent properties and the manufacturing process, the breaking strain in MD is about 1 per cent. Thus it is reasonable to assume that the stress-strain curve of paper follows largely from its network structure [17].

The tensile strength stipulates the maximum stress endurance, but has poor connection to the practical runnability of paper web. The breaks are an issue in spite of the web tensions being of the order of one tenth of the tensile strength. The runnability is linked to local strength variations, and several measurement methods have been suggested [18–20]. Excluding the apparatus malfunctions, paper web breaks are known to originate from microcracks, defects and weak spots. The ability to resist crack initiation from existing flaws is called fracture resistance or fracture toughness. Fracture toughness is known to correlate well with runnability. The fracture toughness determination requires tensile tests

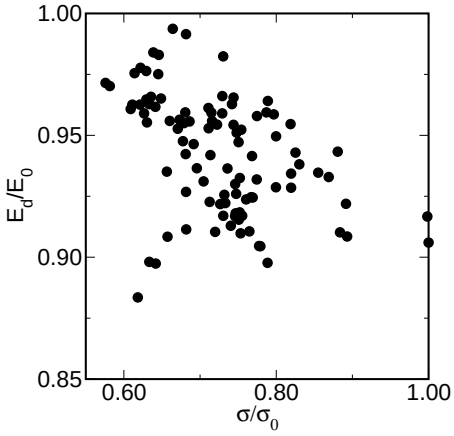

(a) Reloading modulus E_d as a function of relative stress. Machine direction, some machine-made paper grades.

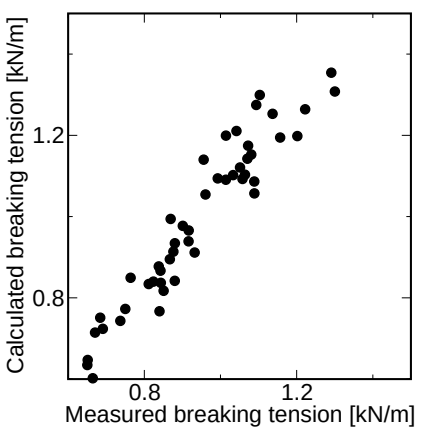

(b) Correlation of calculated (Eq 1.1) and measured apparent tensile strengths [21].

Figure 1.3: Elastic modulus and apparent tensile strength.

with varying notch length. To decrease the experimental work needed, the aim is to be able to calculate the fracture toughness. A theory that originates from continuous medium approximation overestimates the fracture toughness of paper by factor a 30 [21].

During crack propagation elastic energy is released, due to stress relaxation in crack edges. The classical Griffith's criterion states that, in order the crack to grow, released energy must exceed the fracture toughness, the energy demand of fracture in crack tip. Some time ago Morel et al. reported a dependence of released elastic energy on specimen size and surface roughness [22]. Kettunen et al.[23, 24] defined a measure for damage width w in the fracture process zone, and Niskanen[25] introduced an equation for calculating the tensile strength of a specimen with a notch of size a. The engineering equation

$$\sigma_{max} \approx \sqrt{\frac{GE_0}{2\pi(a+w)}}, \tag{1.1}$$

where G is the fracture energy, is a modification of Griffith's criterion and agrees reasonably well with experiments (Figure 1.3b).

Although the strength of paper has been studied widely, there has been very

little information about sample to sample fluctuations . Web breaks are rare events, so for that reason too, the statistical properties of strength are of concern. Strength histograms are helpful to explicate observed values, but they can also reveal something about the underlying processes (Publication I). There are a few theoretical strength distributions that can be compared with experimental histograms. Recently an extensive study of web break statistics was published [26].

Paper is manufactured from dilute water-fiber suspensions. During the dewatering process, inter-fiber water is removed, and also fiber properties change. During drying the fibers shrink more in their transverse direction than in the axial direction. To prevent shrinkage, in the drying process the paper web is held under tension. The tension is higher in machine direction. The low level of transverse tension is the reason for high shrinkage values in CD. The internal stress state is a consequence of drying stresses and proportional to the elastic modulus and the tensile strength. In Publication II the objective was to study the effects of geometrical factors on shrinkage. Anisotropic fiber properties and density give raise to a complicated free sheet shrinkage.

1.3 Fractography

As a material is overstressed, failure takes place, a crack propagates through the sample and a trace of rupture is behind. In a three dimensional body, two fracture surfaces are created. The thickness of paper being small, the surface is almost 1+1 dimensional, and thus the surface is called a fracture line. The crack deviates from a straight path as a result of material heterogeneity. The analysis of fracture trails, fractography, is a common tool to study failure mechanisms in complex materials [27].

The power to resist crack propagation and to cause fracture line winding, relies on the heterogeneity and the micro structure of paper. Traditionally the fracture line is analysed as a height profile $h(x)$. Since Mandelbrot et al. [4] there are numerous attempts to connect fracture roughness to macroscopic energy attributes [22, 28–31]. Roughness is usually measured by an exponent ζ, which is defined by

$$<\delta h>_l \sim l^{\zeta}. \tag{1.2}$$

Here $\delta h$is the standard deviation in height, $<>_l$ the mean over ranges of length l and $\sim$ marks statistical proportionality. Several other methods of fractal analysis

are available too [32–35]. If $\zeta = 1$ the fracture line is self-similar. For $\zeta < 1$ the fracture lines are called self-affine. During the 1990's a consensus of self-affinity of three-dimensional fracture surfaces was reached [5]. The roughness exponent ζ has a universal value 0.8. This value holds for large scales only, above the size of heterogeneities. In the presence of strong disorder the universality hypothesis has not been validated [36]. In two dimensions, for reasons not yet understood, ζ is smaller than in 3D.

The topography of a fracture line can contain some marks of the underlying fracture mechanism characteristic to either 2 or 3 dimensional fracture. Brittle and mostly elastic behavior may produce different fracture lines than very ductile and plastic deformation. It is an open question if the fracture line has any connection to sample strength. Because flaws induce stress concentrations, their size distribution has an influence on the crack path and propagation. In brittle homogeneous media with slow crack velocity, a pure opening mode at the tip is expected [37]. In slow fracture of paper the roughness exponent ζ is found to be independent of strain rate [38]. The faster the crack propagation is, the more the stress concentrates into the crack tip, and the less winding is the fracture line [28]. To discuss these issues 6.5 m long fracture lines of paper webs were analyzed as an example of crack propagation involving disorder (Publication IV).

In a tensile test an increasing fracture localization is produced. In the beginning the fracture is spatially dispersed. During the critical crack growth, most micro ruptures occur in the fracture process zone near the crack tip [25]. In fracture toughness studies, notches of varying length are made in the samples. If the initial notch is long enough, a crack line always initiates from the notch. The fracture line interaction with a single defect as a function of defect size is an interesting and mostly unknown topic. In Publication III notched sample experiments were done to study crack localization in tensile tests. In this thesis dynamical aspects of fractography are not addressed.

1.4 Acoustic Emission

Acoustic emission (AE) is a consequence of rapid release of elastic energy. This energy release originates from micro failures. In the case of paper, it can be a rupture of a bond, a fiber or a combination of these. Elastic energy is first transformed into mechanical oscillations and eventually into heat[39, 40]. Paper failure can be analyzed via acoustic emission, which is a non-destructive method.

Acoustic emission detects intrinsic failures and thus helps to characterize the process [41–43]. It is shown in this thesis by acoustic emission that paper failure has statistical properties similar to those of earthquakes.

The original acoustic emission data is a discretized time sequence of amplitudes $(A_1, A_2, ...)$. Afterwards, the acoustic data is thresholded and divided into separate events (Figure 1.4a). The structure of an event is complex [44] and is usually simply described by its energy. The event energy E is given by $E_i = \sum_j A_j^2$. Also the quiet times $\tau_i = t_{i+1} - t_i$ between the events characterize the sequence of acoustic events. Event duration is typically less than 1 ms and waiting times can last up to 1 s. The typical number of events in a specimen is 1000 - 10000. The individual energies measured are of the order of 1 μJ. Here the analysis focuses on the number of events, event energies, time intervals between events, and their statistics.

Acoustic emission is widely used for industrial monitoring of tanks and leak detection [45]. As a research tool AE is used for detection of Barkhausen noise, in martensitic transformations, wood fracture and testing of reinforced materials [46–48]. An increase in the acoustic emission rate is interpreted as an approaching failure. In paper research acoustic emission was first analyzed by Corte and Kallmess in the late 1960's [49]. They observed accumulation of damage by AE. In the 1990's Yamauchi et al. developed the technique further and reported that fiber and bond breakages can be distinguished by amplitude differences [50]. There are two observations supporting the separation technique [51, 52]. Later Yamauchi et al. reported AE source location detection in paper [53]. Due to technical difficulties and high attenuation [54, 55], the accuracy of the method is not sufficient to study fracture propagation [56, 57]. Recently Houle and Sethna have studied the crumbling noise in paper [58]. In addition to earthquake analogies, this thesis shows that the acoustic energy accumulation during a tensile test has roughly an exponential form (Figure 1.4b).

Earthquake is a complicated spatiotemporal failure phenomenon. Charles Richter developed a way to measure the size of earthquakes. On the Richter scale the magnitude M is proportional to the logarithm of the maximum amplitude of the Crust's motion. The size of an earthquake is thus quantified by the released energy. In the 1950's Richter and Beno Gutenberg posed their empirical law for the size distribution of earthquakes [11]. The law states that in a certain area the number of earthquakes of size M is proportional to $M^{-\beta}$. The parameter β is nearly constant, the reported values in the literature vary usually in the range

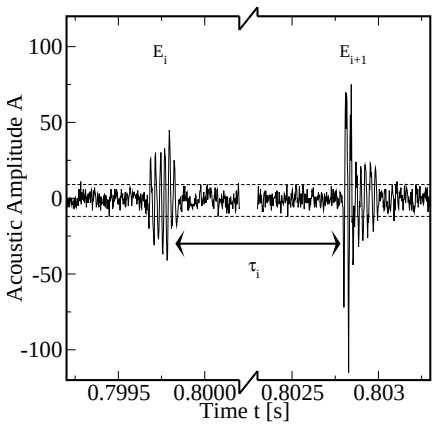

(a) An example with two acoustic emission events. The dashed lines denotes the threshold levels.

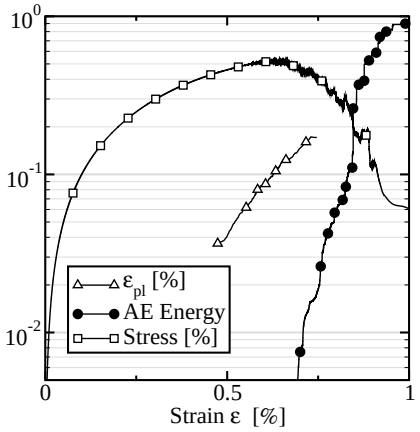

(b) Plastic elongation ϵ_{pl} and cumulative acoustic energy. Curves are averages over 10 specimens.

Figure 1.4: Acoustic emission data.

of 0.8 – 1.2 [59].

Temporal correlations between earthquake events are expressed by Omori's law [12]. In fact this relation is only valid for the aftershocks [60]. Although reliable evidence is lacking, a commonly held belief is that aftershocks are caused by a different relaxation mechanism than the main shocks. Omori's law states that the probability distribution $P(\tau)$ of the quiet time intervals τ is given by

$$P(\tau) \sim \tau^{-\alpha}. \tag{1.3}$$

The waiting time exponent α has a constant value close to 1.0. Similarly, the Gutenberg-Richter law can be expressed in the form

$$P(E) \sim E^{-\beta}. \tag{1.4}$$

In Publications V and VI the energy and waiting time distributions are studied in paper, and in particular the exponents α and β are analyzed.

This resumé presents an overview of the subject matter and the actual scientific contribution can be found in the enclosed Publications I – VI. Chapter 2 is concerned with the strength and Chapter 3 with fractography. The topic of the fourth Chapter is the acoustic emission technique and the results found for paper. Finally, Chapter 5 concludes the thesis.

Chapter 2

Paper Strength

In most applications paper serves as a support for information or as a package of another product, so strength is a useful property. This Chapter is concerned with both the strength and the impact of drying on it. The tensile strength distribution is measured and agreement with theoretical strength models is analyzed. Geometrical effects in shrinkage are modeled and compared with literature.

The strength of paper depends on several important aspects. Due to the multitude of phenomena, no commonly accepted theory of paper strength has been reached yet[1]. A great many models have been proposed, and earlier models emphasize the characterization of a typical fracture element. Lately theories have gradually begun to take into account also the disordered structure of fiber networks[8].

The essential work in fiber furnish and refining optimization cannot nowadays be done by models thus here experimental work is still well-founded. Then again effects of the network structure on the elastic properties can be studied well by computer simulations[61–63]. The properties like voids and bulk related to layered 3-d structure of paper are determinable by analytical and modern computer models too[64–66].

The strength distribution of standard tensile test strips was resolved in Publication I of the thesis. The aforementioned drying induced stress-state of the fiber network has a qualitatively known role in the tensile properties of paper. The effects of the geometry of the network structure on shrinkage can be studied by computer simulations. The simulation results reported in Publication II justify the earlier results [67, 68].

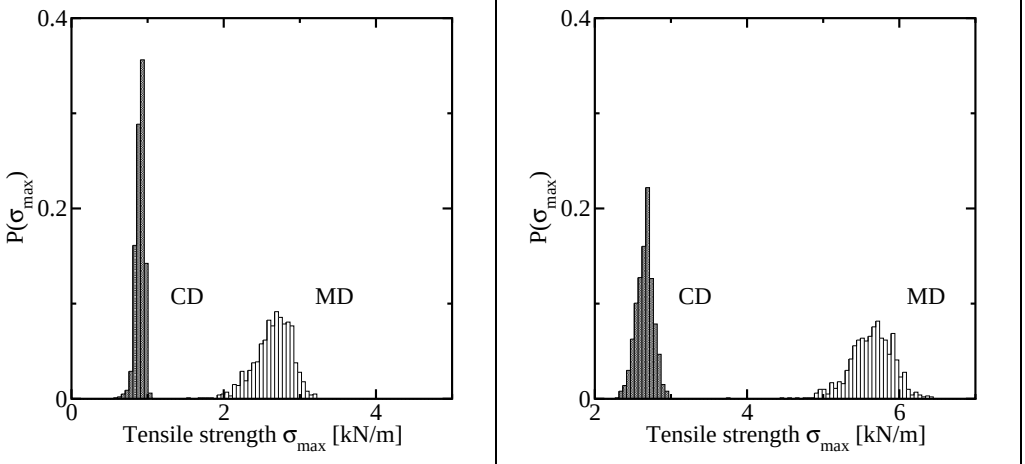

(a) Newsprint paper, CD (shaded) and MD.

(b) Copy paper, CD (shaded) and MD.

Figure 2.1: Distributions of tensile strength σ_{max}. Bin width is 0.05 kN/m.

2.1 Strength Distribution

The statistics of paper strength has been partially unresolved. Strength is related to defects' size and spatial distributions. Here data of tensile tests were obtained for four sets of samples, and the resulting tensile strength histograms were analyzed.

The commercial motivation for decreasing basis weight of paper while preserving its satisfactory strength is resource saving. This aim has its ecological benefits, too. Secondly increasing web velocities in converting technology lead to higher web tensions, and give thus a reason for strength improvement.

The most intuitive model to describe strength is a fiber bundle model that has a global load sharing. In this model the external load σ is shared by all the fibers, and as the failure threshold of the currently weakest fiber is reached, the stress is redistributed among the remaining fibers. In practice global load sharing applies to some brittle systems. The failure threshold in the weakest elements is decisive for the resulting strength. The ductile limit can be described by local load sharing models, in which load excess is dispensed to the neighboring elements only.

We studied the effect of brittle versus ductile material behavior on the strength

statistics in paper. Stress-strain tests of 100 mm long and 15 mm wide strips of paper were conducted using a strain rate $\dot{\epsilon}$ of 100 % min^{-1}. In all 67 $\times$ 15 specimens were measured of newsprint and copy, both in MD and CD. The cumulative density function (CDF) of strength was explored in the four cases (Figure 2.1). These experimental distributions were compared with known theoretical distributions. In the case of strength the candidates are the Weibull distribution

$$P_W(\sigma) = 1 - \exp\left[-\left(\frac{\sigma - c}{\beta}\right)^{\alpha}\right], \tag{2.1}$$

where $\sigma \geq c$ with $\alpha > 0$, $\beta > 0$ and $c \geq 0$, and the recently introduced double exponential strength distribution by Duxbury et al. [69, 70],

$$P_D(\sigma) = 1 - \exp\left[-\exp\left[-\alpha\left(\frac{\beta}{\sigma - c} - 1\right)\right]\right], \tag{2.2}$$

where $\sigma > c$, with $\alpha > 0$, $\beta > 0$ and $c \geq 0$. Both distributions assume an elastic medium, and an essential difference between them is the flaw size distribution. In Duxbury's distribution an exponential distribution is assumed. The Weibull distribution, which is a consequence of an algebraic flaw size distribution, has been observed in various strength related studies [71, 72].

The fits of Weibull and Duxbury distributions are practically indistinguishable from each other and also in apparent agreement with the measurements. In addition, the estimated parameters are almost the same for these two distributions. Both test distributions fail to describe the very low strength tail. Extremely low values are more frequent than predicted by the models. An explanation of this disagreement can be sample misalignment, which results in exceptionally low strength values.

The Publication I concludes that, based on the Kolmogorov-Smirnov [73] (KS) fit goodness test, 6 of the total 8 fits are acceptable, but the χ^2-test accepts only 3 of the 8 cases. Lately Wathén[26] has pointed out an improper use of fit goodness tests in Publication I. This is due to the fact that the Kolmogorov-Smirnov test is a non-parametric test [74], and cannot be preferred to the χ^2-test. Moreover, KS-test suits well small sample number and 1005 specimens cannot be considered a small number in this context. Unfortunately that mistake lead to an incorrect conclusion of exponentially distributed microcracks. The correct result based on the experiments is that the distribution of flaw sizes can be as well algebraic as exponential, if paper is considered as a brittle material.

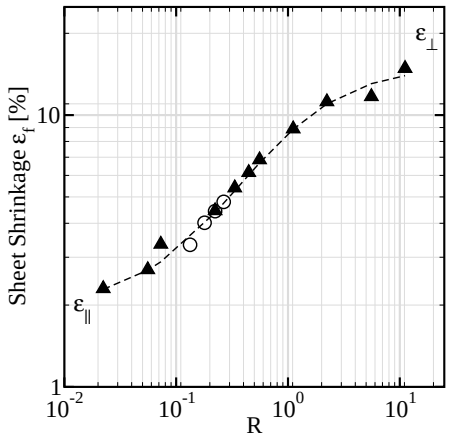

(a) Analytic (Equation 2.3, dashed line) and simulated (circles and triangles) free sheet shrinkage ϵ_f as a function of R.

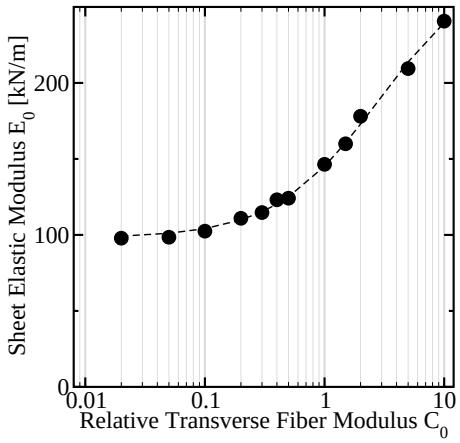

(b) Analytic (dashed line) and simulated (circles) sheet elastic modulus E_0 against relative transverse fiber modulus C_0.

Figure 2.2: Free sheet shrinkage and elastic modulus.

2.2 Structural Effects in Network Shrinkage

Several mechanical properties like the elastic modulus and the strain at break are proportional to internal stress [9]. The internal stresses in paper are mainly induced in drying. Shrinkage in a fiber network was studied using Monte-Carlo simulations. The effect of network density and anisotropic fiber properties on sheet shrinkage, elastic modulus and segment strain distributions were explored.

In machine-made paper part of shrinkage is usually prevented to modify the loading behavior. Shrinkage restraining is the major reason for the MD/CD discrepancy. The qualitative mechanism of drying shrinkage is well-known, but the geometrical aspects of shrinkage to macroscopic properties relationship have not been considered earlier. It is characteristic of internal stresses that their macroscopic average is zero and yet local stresses, compressive and tensile, inside the network can be substantial.

The fibers in the simulation networks considered in this thesis had for generality uniform random orientation and positions. The network of size 1.2 mm $\times$ 1.2 mm consisted of straight fibers with length 1 mm, width $w = 35$ μm and line density $q = 30 - 60$ mm^{-1}. The two-dimensional network had a rectan-

gular inter-fiber bond at every crossing of two fibers. The simulated sheets had a one-layer structure, thickness equaling to fiber thickness. The deformations and equilibrium of the network were solved using a finite element (FE) code by Heyden[75, 76]. The axial fiber modulus $E_{\parallel}$ was set to be 35 GPa and $C_0 = E_{\perp}/E_{\parallel}$ defined the ratio of axial to transverse modulus. The longitudinal drying shrinkage potential of the fibers was taken to be $\epsilon_{\parallel} = 2$ % and the transverse shrinkage potential was $\epsilon_{\perp} = 20$ %. These values are realistic for paper making fibers. Only the difference $\Delta\epsilon = \epsilon_{\perp} - \epsilon_{\parallel}$ influences the internal stresses of the network. To mimic the shrinkage in MD and CD, two shrinkage cases were considered, zero macroscopic shrinkage and free macroscopic shrinkage.

Simulation results for the free shrinkage ϵ_f are shown in Figure 2.2a. The $\epsilon_f(C_0)$ and $\epsilon_f(q)$ data sets collapse when plotted against $R = \frac{C_0 w}{l_s}$, where l_s is the mean segment length. The motivation for this dimensionless quantity arises from mean field arguments. The macroscopic fiber network shrinkage is $\epsilon_f = \epsilon_{\parallel} + \frac{R}{R+1}\Delta\epsilon$. According to this approximation the free shrinkage of the network should be equal to the longitudinal fiber shrinkage plus a term that arises from the transverse fiber shrinkage. The simulated shrinkage values are not quite equal to this expression. Instead they can be reproduced with a slightly modified expression,

$$\epsilon_f = \epsilon_{\parallel} + 0.72\frac{R}{R+1}\Delta\epsilon, \tag{2.3}$$

shown by the dashed line in Figure 2.2a. Thus the dimensionless quantity R encompasses all the effects of network structure (such as density) and fiber elastic properties on sheet shrinkage. Also, the contribution of fiber shrinkage to sheet elastic modulus E_0 can be calculated(Figure 2.2b).

The simulated network shrinkage ϵ_f agrees qualitatively with Equation 2.3 that is motivated by a simple mean field approximation equivalent to the theory of Uesaka [67]. The simulated segment strain distributions are similar to those found in the experiments of Nanko and Wu [68] (Figures 2.3 and 2.4). If the network shrinkage during drying is decreased the paper behavior becomes more brittle. This is due the fact that in the restrained sheet more fiber segments carry load at the same time.

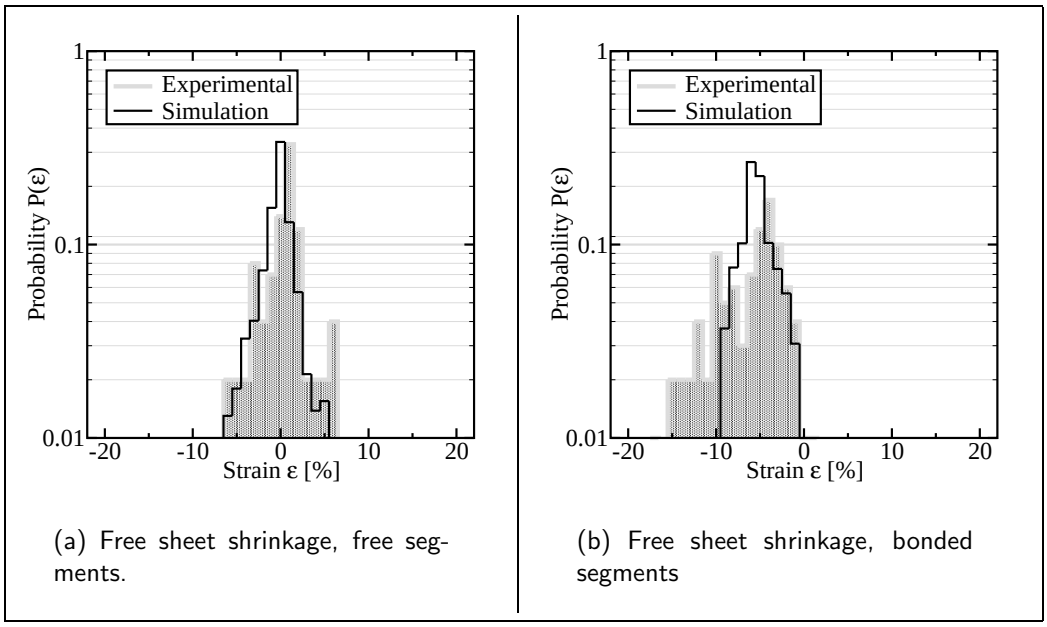

(a) Free sheet shrinkage, free segments.

(b) Free sheet shrinkage, bonded segments

Figure 2.3: Comparison of segment strain histograms in experiments (gray line) and simulations (black line) for a freely dried sheet.

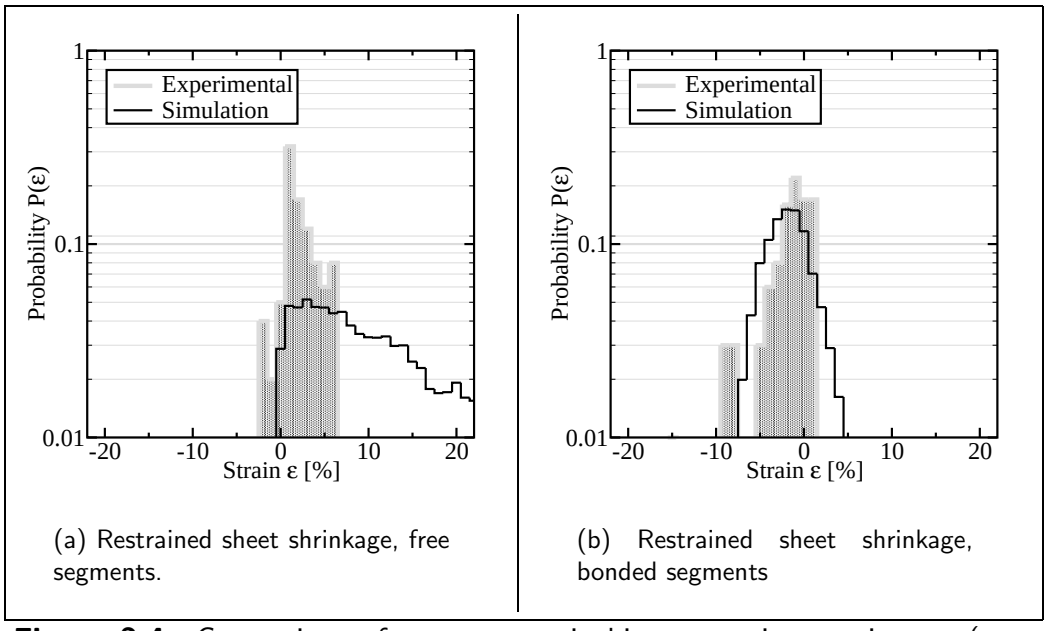

(a) Restrained sheet shrinkage, free segments.

(b) Restrained sheet shrinkage, bonded segments

Figure 2.4: Comparison of segment strain histograms in experiments (gray line) and simulations (black line) for a restrained sheet.

Chapter 3

Fracture lines

Next the focus is set on crack line localization and topography in paper fracture. During the fracture a crack propagates through the medium, whose load carrying capacity vanishes. The process is partly based on energy minimization. The morphology of the fracture line relates to defects and material structure. The fracture process characterization is of general physical interest, too. Here the self-affine nature of fracture line is analysed in paper and pinning, i.e. crack blocking probability, is studied.

It is an open question how cracks develop and interact in real materials and what is the fractal nature of failure trail in the presence of disorder [3–5]. There are several sources affecting the crack path progress. In the microscopic scale the discrete structure affects the drying induced stress concentrations in fiber crossings [8]. At fiber lengths and above, local mass non-uniformity, flocculation, causes elasticity and thus also stress fluctuations. Paper contains micro-cracks, so their coalescence modifies the energy costs in fracture.

Fracture can proceed as a single crack or in a dispersed way as several microcracks. There can also be several macroscopic cracks during the fracture process, the directions of the crack tips can be opposite and their velocities can be inequal. All together these produce oblique load modes and result in crack branching. Even though paper has a non-zero thickness, in fracture the behavior in large scales can be analogous to that of plane rupture. Dynamical effects can produce apparent crack tip inertia [3]. Due to that rupture can involve crack oscillations.

Paper is brittle and catastrophic crack propagation is often witnessed. Rapid rupture is a consequence of elastic energy stored in the network. The upper

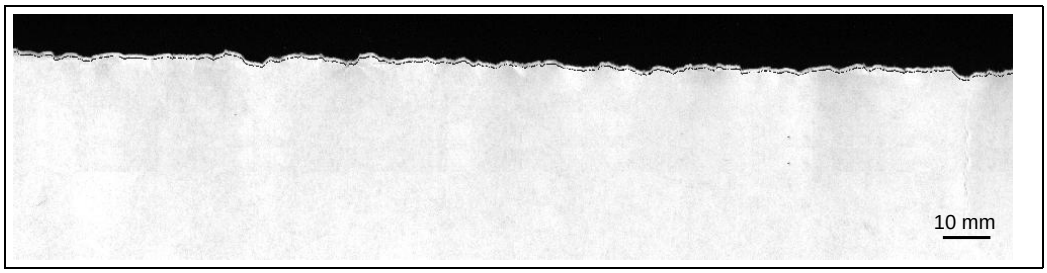

Figure 3.1: Example of a crack line image demonstrating small crack line meandering. Image width is 210 mm.

limit of crack propagation is the Rayleigh velocity, which in the case of paper is approximately 3 km/s.

An initial notch is a common way to promote stable crack propagation. For a small notch intrinsic defects often outdo the applied incision. If the notch is large enough, the fracture path is forced to include the initial notch. An event or position that advances the crack is called depinning, and crack obstruction is called pinning. The incision effect is linked also to the stress interaction range in fracture. In the course of failure there is competition between local and global minimization. The shorter is the interaction length the less the initial notch affects. The significance of an initial notch can be evaluated by the depinning probability, that the crack path goes via the applied incision. That probability can be determinated as a function of notch length a. With a fixed notch length, the more local process the fracture is, the smaller is the probability $P(a)$. The form of $P(a)$ tells when the initial notch is inconsequential. Experiments on notched samples and comparisons of $P(a)$ to theory are presented in Publication III.

The topography of the trail left by the paper rupture involves fluctuations on several length scales (Figure 3.1). Thus statistical description suits well to fractography. There might be size or position dependence in crack fluctuation. Behavior on different length scales is tied to self-similarity of self-affinity. Interpretation of fracture experiments is complex [5, 77, 78], and the determination of the roughness exponent is sensitive to imperfections in the data [32, 33]. Mutual understanding exists about self-affinity, on large scales in 3d the roughness exponent is about 0.8. On short length-scales the exponent is close to 0.5. An example of an in-plane fracture roughness is the values 0.55 and 0.63 reported for plexiglass by Delaplace et al.[79, 80]. In paper self-affinity of crack line was first measured by Kertezs at al., but samples were small and resulted in a wide range of exponents (0.62 – 0.72) [81]. Also Balankin et al. have

reported a multitude (0.52 – 0.82) of roughness exponents for carton and paper [38, 78, 82, 83]. Theoretically the crack path can be modeled by a random walk process. With equal step probabilities and lengths, this model produces a roughness exponent 0.5. Most fracture lines have a tendency not to change direction after each step since the experimentally observed roughness values are above $1/2$. Nothing is known of roughness in fast failure, including that of paper. Publication IV presents analysis of long unstable fracture lines in paper.

3.1 Crack pinning

The main objective was to study the probability of crack pinning via an initial crack. These were applied to tensile test strips (100 mm $\times$ w = 100 mm). The length of the edge notch was a and it was perpendicular to the applied stress. The notch lengths were measured with an accuracy of 0.05 mm and tallied into 5-8 categories. The standard deviation of notch length within a category was in a range of 0.2 mm.

In general, for ideally elastic media the stress σ in the vicinity of a crack tip is obtained by

$$\sigma(r, \theta) \sim \frac{g(\theta)}{\sqrt{r}}, \tag{3.1}$$

where r is the distance from crack tip and θ the polar angle. On the average the crack propagates in the direction perpendicular to the external load, where the function g is the largest. Equation 3.1 diverges as $r \to 0$, and describes a very brittle behavior. In practice plastic deformations limit the stress and give rise to crack pinning. The plastic zone corrections were studied by Donner [84], and the resulting equation is analogous to Equation 1.1. Obviously this equation gives just the stress enhancement at the crack tip, and the stress level depends also on the global load and the remaining ligament length. Thus experiments with variable notch length can be used to study the plasticity and crack tolerance in paper. To interpret the experimental results, the function $P(a/w)$ is defined as the fraction of crack lines going through the initial notch.

The results show that an initial notch length of 3 % was big enough to be always in the final crack line. Correspondingly a 0.5 % notch had no practical significance. This length of the smallest contributing notch a_{min} gives a scale to paper inhomogeneity. The measured $P(a/w)$ contain some inaccuracy, but clearly capture the main behavior. Figure 3.2a shows the distribution for

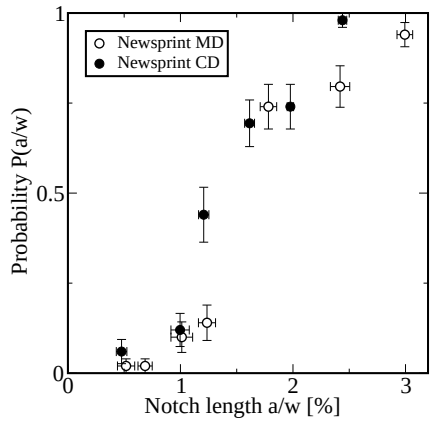

(a) Probability P of the final crack to contain the initial notch as a function of relative notch length a/w.

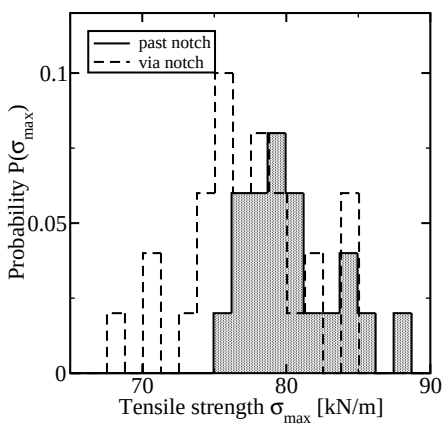

(b) Distribution of newsprint CD tensile strength in pinned (past notch) and depinned (via notch) samples. Mean values differ with 97.5 % probability.

Figure 3.2: Depinning fraction $P(a/w)$ and strength distributions for newsprint.

newsprint paper. The transition from $P = 0$ to $P = 1$ is clearly monotonic and close to linear around $P(a/w) = 0.5$.

If the final crack is taking advance of the initial notch the tensile strength of the sample is expected to diminish. Thus the tensile strength averages in depinned (crack initiates from notch) and pinned samples were compared for newsprint CD. The mean value for the cracks that go past the initial notch was 80 kN/m. For the cracks passing through the notch the average was 77 kN/m. The standard deviation was in both cases 5 kN/m. The mean values were different with a 97.5 % probability (Figure 3.2b).

3.2 Geometrical Fracture Line Analysis

The morphology of long fracture lines in paper samples was also examined, and self-affine rupture lines were observed.

Three 6.5m wide paper webs were broken in paper machine. Two of the samples

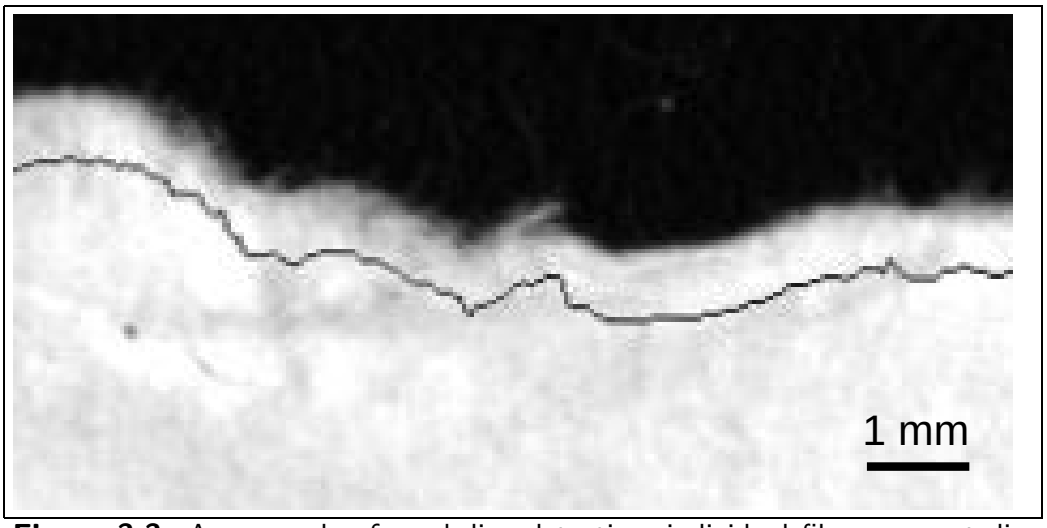

Figure 3.3: An example of crack line detection, individual fibers are not distinguishable. Image width is 10 mm. The detected edge is marked by the dark line which is shifted for clarity.

were from the same machine. The third sample (sample 2) was from another machine using however the same raw material. The duration of the rupture was less than 1 s and the rupture was unstable. Fast cracks would be expected to be smooth due to stress concentration.

Each crack line was scanned with a flatbed scanner in about 30 pieces (similar to Figure 3.1). The crack line was detected from the images by gray level thresholding. The crack lines consisted of about 160 000 points. The pixel size was 42 μm, so individual fibers could not be distinguished (Figure 3.3). The branching of the crack lines was modest. They were analysed as a 1-d series $h(x)$, and the main objective was to study their self-affinity. Also other analysis methods were introduced and applied. In length-scales comparable to fiber width, the fracture process is three dimensional [23].

The crack line roughness in length scales 1 – 1000 mm was analysed by five methods. For the roughness exponent ζ we obtained 0.64$\pm$0.03, 0.54$\pm$0.04, and 0.65$\pm$0.02 for samples 1,2, and 3, respectively (Figure 3.4). On smaller scales the topography of the fracture line was not resolved. The error values are not based on fit inaccuracy but on variation between the method used and on sensitivity studies. Regardless of the analysis method, the sample 2 had a ζ value about 0.1 smaller than those for samples 1 and 3. It is a matter of taste whether one considers all the samples to have the same exponent, or that in sample 2 the exponent is significantly lower and close to the random walk exponent $1/2$. The

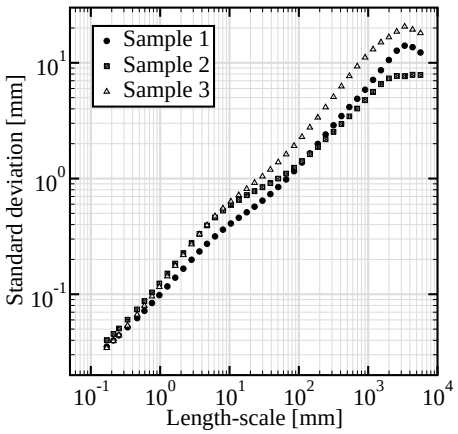

(a) The standard deviation method. Roughness exponents are $\zeta = 0.63 \pm 0.03$, 0.53 ± 0.02 and 0.665 ± 0.009 for samples 1,2 and 3, respectively.

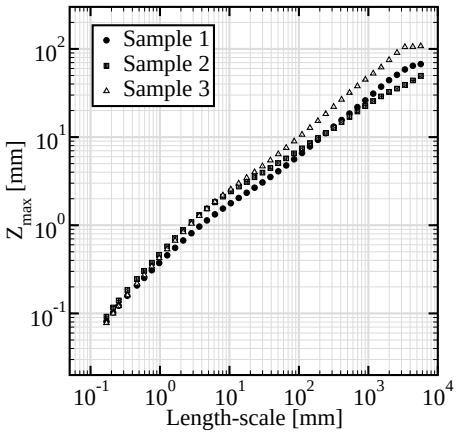

(b) The maximum difference method. Roughness exponents are $\zeta = 0.634 \pm 0.007$, 0.53 ± 0.02 and 0.664 ± 0.004 for samples 1,2 and 3, respectively.

Figure 3.4: Crack line roughness by two methods.

length of monotonic fracture line sections has an exponential distribution for a random walk process. In paper fracture long (over 1 mm) monotonic sections are more frequent. For unknown reason the cracks seem to have an increased probability to maintain their current direction. Finally, the scaling curves show systematically a bump in the range 5 – 20 mm, possibly originating from density correlations in paper [85].

Chapter 4

Acoustic Emission Spectroscopy

Paper fracture was also studied via acoustic emission (AE) analysis, and results are reported for tensile and peel-in-nip test AE experiments. Microscopic avalanches of acoustic energy were observed. In tensile tests, the acoustic emission energy and the waiting times between acoustic events follow power-law distributions. This observation remains in force irrespective of strain rate in the range 0.1 – 100 %/min. In peel paper splitting two power-law behaviors, different from the tensile test case are observed. Differencies in fracture process between the standard tensile test and peel test are discussed.

The behavior resulting in a power-law dependence is likely to be independent of any details, thus comparison between acoustic emission and earthquakes is a valid idea. The event energy spectrum in a fracture process is described by the Gutenberg-Richter-law (Equation 1.4) with an exponent β. Correspondingly the Omori's power-law (Equation 1.3) relates an exponent α to the waiting time distribution $P(\tau)$ between the rupture events. Several experimental observations of both Gutenberg-Richter's and Omori's power-law exist [41, 57, 86, 87]. Very often these laws appear simultaneously [86, 87]. However, since the origins of these power-laws are unknown, also the possible connection between them is unknown [59, 60]. Especially the physical origin of the time-to-failure statistics is missing. Fracture models that include temporal aspects can be grouped into two classes: dynamical ones, which involve deterministic stress transfer [88–90], and statistical models in which probabilities generate the time dependence.

When a material that breaks responds to a changing external load by impulsive events, and the distribution of released energy is a power-law, it indicates that there is no typical event size. For a system with non-local elastic interactions

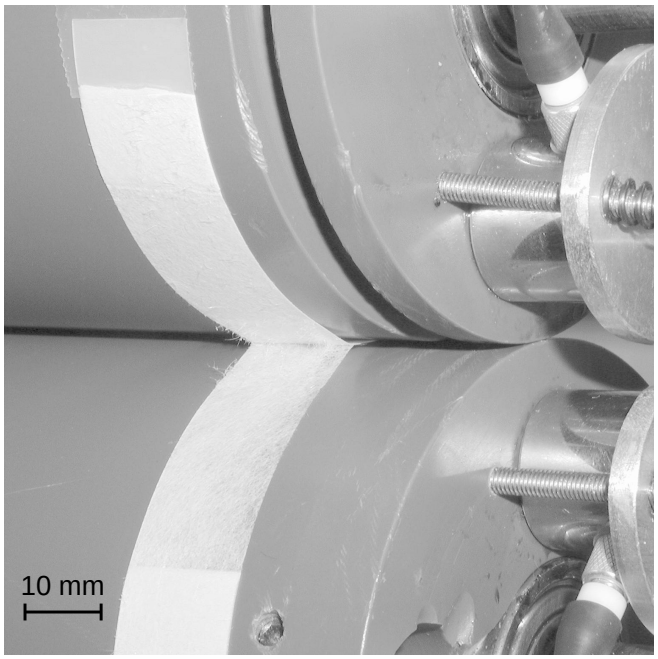

Figure 4.1: Photograph of the peel-in-nip device, roll diameter is 80mm.

mean field arguments lead to an exponent $\beta = 1.5$ [90]. In the case of granite Lockner et al. reported experimental observation of exponent β changes during a compressive fracture [57]. In the pre-failure regime of granite fracture β is above 2, at the maximum stress β lowers close to 1.0, and after that it recovers to $\beta \approx 1.8$. Yamauchi and Murakami observed as a function of strain a linear increase in optical reflectance, and a roughly exponential increase in the cumulative AE counts. They concluded that, in tensile fracture of paper, two different types of structural change are present [52]. In mode I fracture experiments Garcimartín et al. reported $\beta \approx 1.5$ for chipboard wood plates, and 2.0 for fiberglass. They also suggested that rupture can be viewed as a critical phenomenon or a phase transition [91, 92]. In paper crumpling β is approximately 1.3 [58].

The peel-in-nip test is a new method for paper testing[93], in which z-directional failure takes place in the vicinity of a nip (Figure 4.1). The front end of the specimen is attached to both of the rolls, and the cylinders are then reeled by hand to initiate the peeling. Thereafter cleavage proceeds based on equilibrium of three supporting forces. Opposite to the tensile test, in the peel-in-nip test the length of the crack line is large compared with the fiber length and the average crack line position is stationary in relation to the rolls. Therefore large

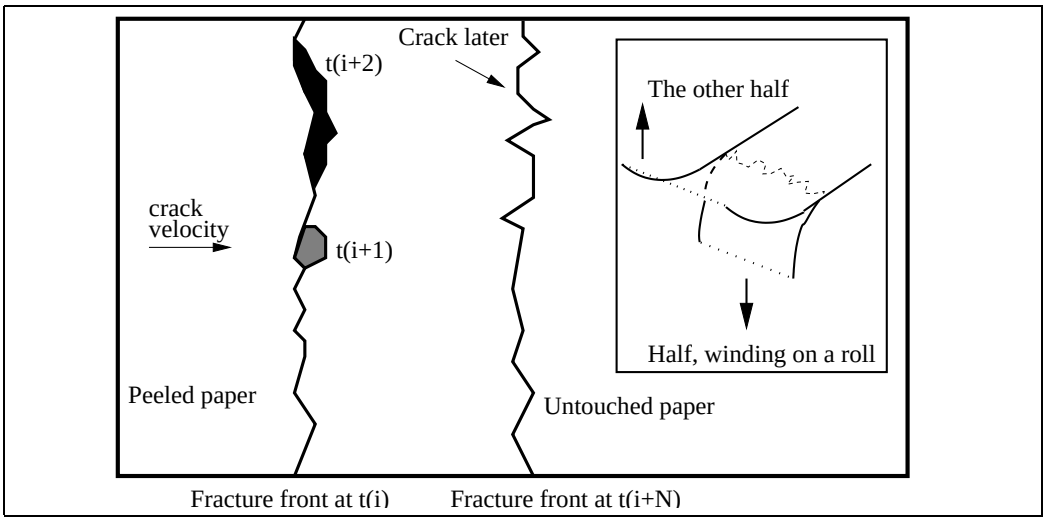

Figure 4.2: Fracture propagation in the peel-in-nip test.

fracture surfaces can be produced. In the standard tensile test the fractured area per strip is about 1 mm^2, and in the peel-in-nip test over 100 mm^2.

In the peel-in-nip test the stress geometry is three dimensional and stress is cut off quickly with increasing distance from the average crack line position. The length (parallel to the roll velocity) of the avalanche is presumably close to constant, only the width of the avalanche is varying (Figure 4.2). Most events take place apart from the preceding event and thereby in a sense initiate a new crack-tip. Because the avalanche energy is expected to be proportional to the fractured area, the acoustic emission can be used to monitor the avalanche areas during the fracture.

In different strength tests the rupture processes involve different timescales. In the classical tensile test two regimes can be distinguished (Figures 1.4b and 4.4a), the pre-fracture phase, where behavior is nearly elastic and cracking disperse, and the second phase that takes place after stress maximum. During the second phase the dominating crack is propagating in a continuous way, crack branching is very low, and most failures are in the so called fracture process zone (FPZ). The FPZ comprises the crack-tip and its vicinity[24]. In the peel-in-nip test fracture is stable, and the acoustic emission activity is roughly constant. Thus very long waiting times cannot be expected. Opposite to the tensile test, the AE event sizes in the peel-in-nip have no tendency during the test.

4.1 Experimentation

Acoustic emission is ultrasonic ($f \sim 1$ kHz$-$ 10 Mhz) mechanical oscillation. In general wave propagation in disordered media is a complex subject[54–56, 94–98]. The waveform of acoustic emission varies heavily, due to many modifying effects like frequency dependent attenuation, interference due to internal structure and sample boundaries, dispersion and piezo hysteresis. Although the collective wave deflection may be strong, we assume that for typical events the variation of attenuation is small. It is however true that differences in the origin of acoustic emission may cause significant sample-to-sample variation.

The AE system consisted of a piezo electric transducer, a pre-amplifier and continuous data-acquisition. The primary instrument detecting ultrasound acoustic emission was the piezo electric transducer. The transducer transformed mechanical motion to voltage. The data acquisition in AE experiments was continuous and done by a 12-bit AD-card in a Pentium PC. The experiments in Publication V were made with a single AE-channel with the data acquisition rate 100000 samples/s (Figure 4.4). In that case the amplifier also included a rectifier. In Publication VI two bi-polar AE-channels were recorded at a rate of 400000 samples/s (Figure 4.3). During the test the raw data was stored in the computer. Afterwards the events were detected from the time series by an amplitude thresholding method [58, 99].

4.2 Tensile Fracture

To study the time dependent features of paper AE newsprint samples were tested in the machine direction with a mode I laboratory testing machine of type MTS 400/M. Due to the lack of constraints, the samples could also have out-of-plane deformations. The sample dimensions were $l = 100$ mm and $w = 100$ mm, the length of an initial notch was 15 mm, and the deformation rate $\dot{\epsilon}$ varied between 0.1 %/min and 100 %/min. For these strain rates the sound velocity timescale is much faster than that implied by $l/\dot{\epsilon}$.

Figure 4.4a shows an example of two tests under strain control. Stress-strain curves have typically two parts: pre-failure which is almost elastic up to the maximum stress, where the final crack starts to propagate, and a tail that arises due to the cohesive properties of paper, which allow for stable crack propagation. The faster the strain rate the less is the role of the tail. For the smallest strain

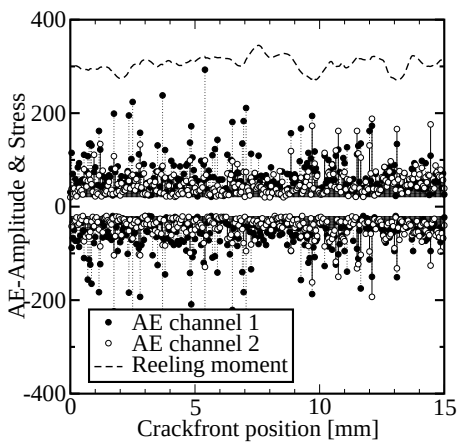

(a) Acoustic emission data and reeling moment from a peel-in-nip test. Signal thresholding is illustrated by the white section in the middle.

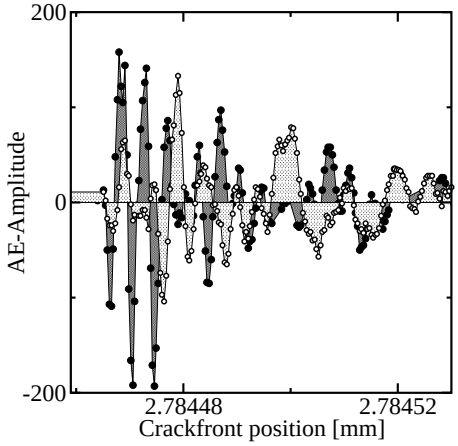

(b) An acoustic event as detected by two piezo transducers.

Figure 4.3: An example of the data from the peel-in-nip test.

rate (0.1 %/mm) most of the AE originates from the tail (more than 90 %), while for the highest strain rate (100 %/min) the situation is the opposite. Quantities of interest are the statistical properties before the maximum, after it, and the integrated totals, in particular the energy distributions.

The energy histogram $P(E) \sim E^{-\beta}$ has an exponent $\beta = 1.25 \pm 0.10$, and the waiting times an exponent $\alpha = 1.0 \pm 0.1$. Within the measuring accuracy, both exponents are independent of the strain rate. The energy exponent β is almost the same in pre- and post-fracture parts of the stress-strain curve (Figure 4.4b). These results do not compare well with fracture models, and the tensile test results leave open the origins of the observed scalings. The reported Gutenberg-Richter power-law exponents β vary from 1.2 to 1.5 [41, 58, 90, 91], but exponent α for Omori's law is mostly ~ 1. Acoustic emission was also simulated in random fuse networks with the result $\beta \approx 1.7$ [43], and in a dynamical spring network with the same results [89].

In a tensile test external energy is continuously fed in, but the fracture process is not an example of self organized criticality or phase transition. There is very little predictability or correlations in the time series of acoustic events. However, it seems that large and long events are separated, on the average, by shorter intervals from the neighboring events. The plastic deformation accruing above

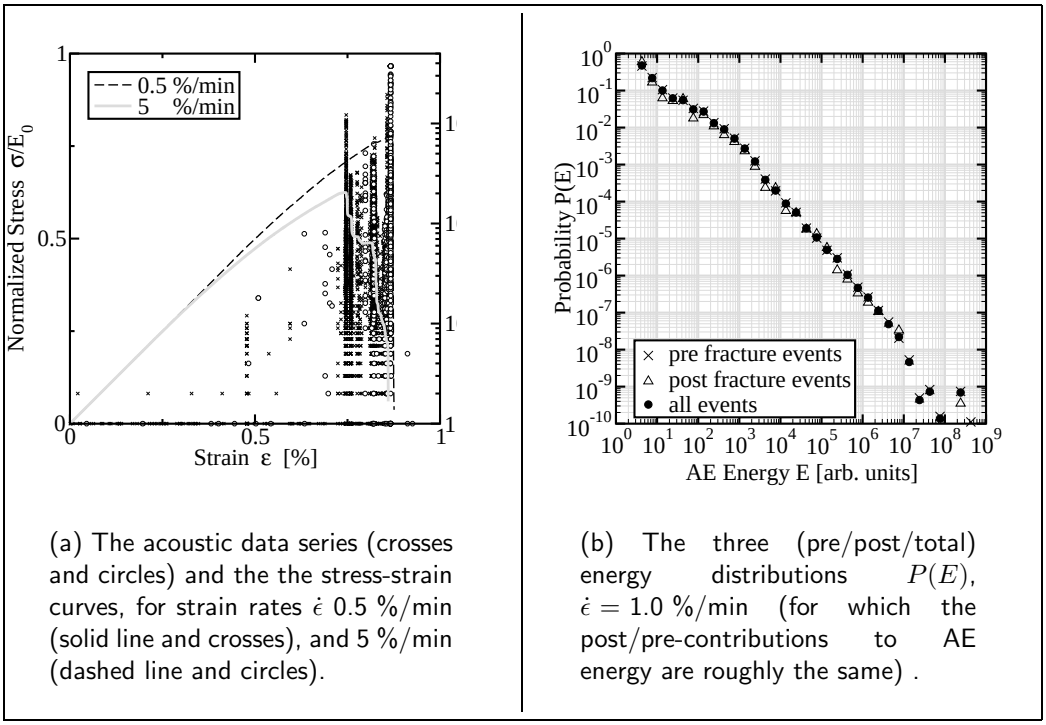

(a) The acoustic data series (crosses and circles) and the the stress-strain curves, for strain rates $\dot{\epsilon}$ 0.5 %/min (solid line and crosses), and 5 %/min (dashed line and circles).

(b) The three (pre/post/total) energy distributions $P(E)$, $\dot{\epsilon} = 1.0$ %/min (for which the post/pre-contributions to AE energy are roughly the same) .

Figure 4.4: Acoustic emission in the tensile test.

a strain of 0.5 % [100] increases exponentially, as does the acoustic emission energy (Figure 1.4b).

4.3 Peel Fracture

Tensile tests in Publication V pointed out wide scale-free distributions of acoustic energies and waiting times. To study these phenomena, further experiments were carried out on the peel-in-nip. In peel-in-nip fracture the process is stable and has translational invariance. Thus AE statistics may reveal some new characteristics.

Fracture in peel-in-nip and tensile tests was studied for standard handsheet samples. In both cases small (length 70 mm, width 15 mm) strips were used to reduce the elastic energy, that often leads to catastrophic crack growth. Furthermore, to encourage stable crack propagation, also tensile samples with initial notches (notch length $\approx$ 2.5 mm) were measured. Despite the small sample size and the applied notch, most tensile tests ended abruptly.

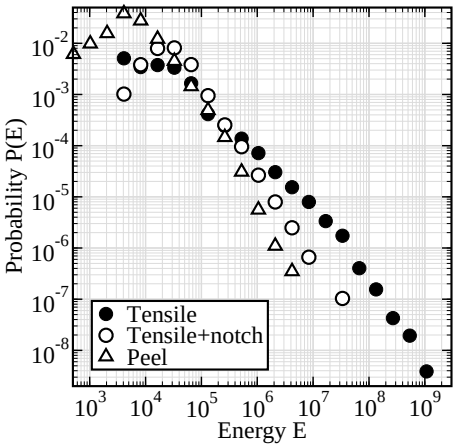

(a) Event energy distributions. Energy exponent is $\beta = 1.2\pm0.2$, 1.7 ± 0.2, and 2.0 ± 0.2 for tensile, tensile with an initial notch, and peel-in-nip tests, respectively.

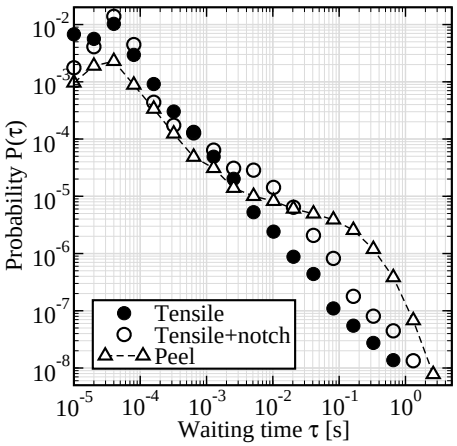

(b) Event waiting time distributions. Waiting time exponent is $\alpha = 1.0\pm0.1$ for the tensile test with and without an initial notch. In the peel-in-nip test the waiting time distribution is not a power-law.

Figure 4.5: Acoustic emission statistics in tensile and peel-in-nip tests.

The waiting time distribution in the tensile tests is a power-law. This remains true for the tensile test with an initial notch, too. In both cases the exponent α is approximately 1.0 (Figure 4.5b). In the peel-in-nip case the distribution deviates clearly from a power-law in the time scale 10 - 500 ms. Decreasing the pulp refining improves slightly the linearity of the distribution in log-log scale [99]. The α values reported in the literature are without exception very close to 1.0 [41]. The mechanism producing this time-to-failure distribution is presumably universal.

The acoustic event energy distribution obeys fairly the Gutenberg-Richter power-law also in the peel-in-nip test. The exponent β was 1.2 ± 0.2 in the tensile tests and 2.0 ± 0.2 in the peel-in-nip tests (Figure 4.5a). In addition the tensile tests with a large initial notch resulted in an exponent 1.7 ± 0.2. However, the accuracy of the slope determination is not sufficient to rule out the possible equality of the exponents for the tensile test with a large initial notch and the peel-in-nip test. Neither is the power-law dependence the only possible form for the observed energy distributions. Incontrovertibly the experiments show that the distributions are very wide, and that events do not have any intrinsic size.

The distinction of exponent β values is very interesting when considered together with differencies in the test geometries. Disperse failure (tensile test) produces quite a small exponent. The value might be an implication of disorder in paper. Localized failure (tensile test with an initial notch) is an consequence of stress enhancement in the crack-tip. This leads to a more narrow energy distribution, and thus to a larger β. The exponent in the in-plane tear test[24] is presumably close to the tensile test with an initial notch. In the experiments reported in Publications V and VI the relative notch length was almost the same ($\approx$ 15 %), but resulted in different exponent β values. This is due to the effect of the fracture process zone around the crack-tip. In together with typical FPZ size (5 mm), the notch length in Publication V was 20 % and in Publication VI 50 %. In the peel-in-nip test crack propagates stably by successive crack initiations of varying width, and results in considerably large number of small events. Hence the exponent β is larger than for the tensile test cases. In addition it seems possible that the properties of the disordered structure of paper do not determine the fracture process in the peel-in-nip test.

The experiments reported in Publication VI show evidence of three distinct exponent values in paper rupture. The observations are in agreement with the fracture localization scheme proposed by Lockner [57]. Power-law AE energy distributions were observed, in disagreement with the proposed bond and fiber breakage classification hypothesis [50, 51]. Based on the results of Tanaka et al. [93] and our AE experiments, we make a proposition that fiber and bond breakages can not be distinguished, and that the detailed properties of the constituents are not decisive for the mechanisms of paper failure.

Chapter 5

Summary

This work consists of a simulation study of fiber network shrinkage, and of experiments on paper strength statistics, fracture line properties and fracture processes.

Tensile strength distributions were studied in four sets of samples. 1005 tensile specimens were measured in each case. The observed strength distributions were found to obey Weibull or Duxbury distributions. Numerical simulations of shrinkage in fiber networks were performed. The effect of network density and anisotropic fiber properties on network stress distributions were explored. The simulated shrinkages agreed with those found in the experiments of Nanko and Wu [68]. The statistics of crack pinning in paper was studied. Tensile tests with an initial notch showed a localization phenomenon. The fracture line geometry resulting from fast failure in paper was measured. The 6.5 m wide samples were found to have a roughness exponent $\zeta = 0.60 \pm 0.05$. However, systematic deviations from pure self-affine behavior were observed.

Acoustic emission was measured in tensile and peel fracture experiments. The energy distributions of the acoustic emission events followed power laws, with exponents $\beta = 1.2 \pm 0.2$ (tensile), $\beta = 1.7 \pm 0.2$ (tensile with an initial notch) and $\beta = 2.0 \pm 0.2$ (peel). The event intervals had a wide distribution, in the tensile tests a power law with exponent $\alpha \approx 1.0$ was observed. In peel fracture the interval distribution was wide too, but superimposed on a scale-free statistics there was also a definite time-scale, related to the average segment length in the fiber network. New microscopic fracture models can benefit from the observed distributions. The results reported also give motivation to further applications of acoustic emission, for instance in creep fracture of paper.

Bibliography

[1] K. Niskanen. In *Products of Papermaking*, edited by C. Baker (Pira International, Leatherhead, United Kingdom, 1993), p. 641. Transactions of the 10th Fundamental Research Symbosium.

[2] R. de Borst. Engineering Fracture Mechanics **69**, 95 (2002).

[3] J. Fineberg and M. Marder. Physics Reports **313**, 1 (1999).

[4] B. Mandelbrot, D. Passoja, and A. Paullay. Nature **308**, 721 (1984).

[5] E. Bouchaud. J. Phys. Cond. Mat **9**, 4319 (1997).

[6] J. Oliver, A. Huespe, M. Pulido, and E. Chaves. Engineering Fracture Mechanics **69**, 113 (2002).

[7] H. Herrmann and S. Roux. *Statistical models for the fracture of disordered media* (Elsevier Science Publishers, Amsterdam, North Holland, 1990).

[8] M. Deng and C. Dodson. *Paper: An Engineered Stochastic Structure* (Tappi Press, Atlanta, USA, 1994).

[9] K. Niskanen. *Paper Physics* (Fapet Oy, Helsinki, Finland, 1998).

[10] R. Seth and D. Page. In *The Role of Fundamental Research in Paper Making* (Mechanical Engineering Publ. Ltd, London, United Kingdom, 1983), p. 421.

[11] B. Gutenberg and C. Richter. Bull. Seismol. Soc. Amer. **34**, 185 (1944).

[12] F. Omori. J. College Sci. Imper. Univ. Tokyo **7**, 111 (1895).

[13] D. Page, P. Tydeman, and M. Hunt. In *Formation and Structure of Paper* (Mechanical Engineering Publ. Ltd, London, United Kingdom, 1962), p. 249.

[14] L. Nordman. In *Fundamentals of Papermaking Fibers* (British Paper and Board Makers Association, London, United Kingdom, 1958), p. 333.

[15] R. Mark, J. C.C. Habeger, J. Borch, and M. Lyne. *Handbook of Physical Testing of Paper*, volume 1 (Marcel Dekker, USA, 2002).

[16] R. Mark, J. C.C. Habeger, J. Borch, and M. Lyne. *Handbook of Physical Testing of Paper*, volume 2 (Marcel Dekker, USA, 2002).

[17] M. Ostoja-Starzewski and D. Stahl. J. Elasticity **60**, 131 (2000).

[18] R. Seth and D. Page. J. Mat. Sci. **9**, 1745 (1974).

[19] P. Wellmar, C. Fellers, and L. Delhage. Nordic Pulp and Paper Research Journal **12**, 189 (1997).

[20] S. Östlund, K. Niskanen, and P. Kärenlampi. J. Pulp Paper Sci. **25**, 356 (1999).

[21] R. Wathén. *Characterizing the Influence of Paper Structure on Web Breaks*. Licentiate's Thesis, Helsinki University of Technology, Department of Forest Products Technology (2003).

[22] S. Morel, J. Schmittbuhl, E. Bouchaud, and G. Valentin. Phys. Rev. Lett. **85**, 1678 (2000).

[23] H. Kettunen and K. Niskanen. J. Pulp Paper Sci. **26**, 35 (2000).

[24] H. Kettunen. *Microscopic Fracture in Paper*. Ph.D. Thesis, Helsinki University of Technology, Department of Forest Products Technology (2000).

[25] K. Niskanen, H. Kettunen, and Y. Yu. In *The Science of Papermaking*, edited by C. Baker (Pira International, Leatherhead, United Kingdom, 2001), p. 1467. Transactions of the 12th Fundamental Research Symbosium.

[26] R. Wathén. *Evaluating Dynamic Strength Properties of Paper with a Pilot Machine*. Master's Thesis, Helsinki University of Technology, Department of Forest Products Technology (2000).

[27] D. Hull. *Fractography* (Cambridge Press, Cambridge, United Kingdom, 1999).

[28] J. Fineberg, S. Gross, M. Marder, and L. Swinney. Phys. Rev. Lett. **67**, 457 (1991).

[29] E. Bouchaud, G. Lapasset, J. Planés, and S. Naveos. Phys. Rev. B **48**, 2917 (1993).

[30] J. Åström, M. Alava, and J. Timonen. Phys. Rev. E **62**, 2878 (2000).

[31] O. Malcai, D. Lidar, O. Biham, and D. Avnir. Phys. Rev. E **56**, 2817 (1997).

[32] I. Simonsen, A. Hansen, and O. Nes. Phys. Rev. E **58**, 2779 (1998).

[33] J. Schmittbuhl, J.-P. Vilotte, and S. Roux. Phys. Rev. E **51**, 131 (1995).

[34] N. Vandewalle and M. Ausloos. Phys. Rev. E **58**, 6832 (1998).

[35] A. Mehrabi, H. Rassamdana, and M. Sahimi. Phys. Rev. E **56**, 712 (1997).

[36] X. Zhang, M. Knackstedt, D. Chan, and L. Paterson. Europhys. Lett. **34**, 121 (1996).

[37] M. Adda-Bedia, R. Arias, M. B. Amar, and F. Lund. Phys. Rev. E **60**, 2366 (1999).

[38] A. Balankin, L. Hernandez, G. Urriolagoitia, O. Susarrey, , J. González, and J. Martinez. Proc. R. Soc. Lond. A **455**, 2565 (1999).

[39] A. Tanaka, Y. Otsuka, and T. Yamauchi. Tappi J. **80**, 222 (1997).

[40] H. Kettunen, A. Tanaka, and T. Yamauchi. In *2000 International Paper Physics* (EFPG, CTP, Tappi Paper Physics Committee, Grenoble, France, 2000), p. 120. 2000 Progress in Paper Physics.

[41] J. Sethna, K. Dahmen, and C. Myers. Nature **410**, 242 (2001).

[42] K. Ono. J. Acoustic Emission **12**, 177 (1994).

[43] J. Rosti. *Acoustic Emission During Tensile Straining of Paper*. Master's Thesis, Helsinki University of Technology, Department of Engineering Physics and Mathematics (1999).

[44] M. Majeed and C. Murthy. J. Acoustic Emission **12**, 107 (1994).

[45] T. Drouillard. *Acoustic Emission, A Bibliography with Abstracts* (IFI/Plenum, USA, 1979).

[46] G. Scott. *Basic Acoustic Emission* (Gordon and Breach Science Publishers, Montreux, Switzerland, 1991).

[47] A. Reiterer, S. Stanzl-Tschegg, and E. Tschsegg. Wood Science and Technology **34**, 417 (2000).

[48] R. Nordstrom. *Acoustic Emission Characterization of Microstructural Failure in the Single Fiber Fragmentation Test*. Ph.D. Thesis, Swiss Federal Institute of Technology Zurich (1996).

[49] H. Corte and O. Kallmes. In *Formation and Structure of Paper* (Mechanical Engineering Publ. Ltd, London, United Kingdom, 1962), p. 351.

[50] T. Yamauchi, S. Okumura, and N. Noguchi. J. Pulp Paper Sci. **16**, 44 (1990).

[51] P. Gradin, S. Nyström, P. Flink, S. Forsberg, and F. Stollmaier. J. Pulp Paper Sci. **23**, 113 (1997).

[52] T. Yamauchi and K. Murakami. Tappi J. **76**, 101 (1993).

[53] T. Fuketa, S. Okumura, M. Noguchi, and T. Yamauchi. J. Acoustic Emission **11**, 21 (1993).

[54] R. Mann. *Elastic Wave Propagation in Paper*. Ph.D. Thesis, Lawrence University, Appleton, Wiscosin, The Institute of Paper Chemistry (1979).

[55] S. de Vries. *Propagation of Transient Acoustic Waves in Porous Media*. Ph.D. Thesis, Delft University of Technology, Faculty of Information Technology and Systems (1989).

[56] F. Beall. Wood Science and Technology **36**, 197 (2002).

[57] D. Lockner, J. Byerlee, V. Kuksenko, A. Ponomarev, and A. Sidorin. Nature **350**, 39 (1991).

[58] P. Houle and J. Sethna. Phys. Rev. E **54**, 278 (1996).

[59] J. Rundle, S. Gross, W. Klein, C. Ferguson, and D. Turcotte. Tectophysics **277**, 147 (1997).

[60] K. Christensen, L. Danon, T. Scanlon, and P. Bak. In *Self-Organized Complexity in the Physical, Biological and Social Sciences* (National Academy of Sciences, Irvine, California, USA, 2002).

[61] V. Räisänen. *Numerical Models for Reversible and Irreversible Deformations of Disordered Media*. Ph.D. Thesis, Helsinki University of Technology, Department of Engineering Physics and Mathematics (1997).

[62] V. Räisänen, M. Alava, K. Niskanen, and R. Nieminen. Nordic Pulp and Paper Research Journal **11**, 243 (1996).

[63] J. Åström and K. Niskanen. Europhys. Lett. **21**, 557 (1993).

[64] M. Alava and K. Niskanen. Phys. Rev. Lett. **73**, 3475 (1994).

[65] E. Hellén, J. Ketoja, K. Niskanen, and M. Alava. J. Pulp Paper Sci. **28**, 55 (2002).

[66] E. Hellén. *Nonequilibrium Dynamics in Fiber Networks, Aggregation and Sand Ripples*. Ph.D. Thesis, Helsinki University of Technology, Department of Engineering Physics and Mathematics (2002).

[67] T. Uesaka. J. Mat. Sci. **29**, 2373 (1994).

[68] H. Nanko and J. Wu. In *International Paper Physics Conference* (Niagara-on-the-Lake, CPPA and TAPPI, Canada, 1995), p. 103.

[69] P. Duxbury, P. Leath, and P. Beale. Phys. Rev. B **36**, 367 (1987).

[70] P. Duxbury, P. Leath, and P. Beale. Phys. Rev. Lett. **57**, 1053 (1986).

[71] Z. Bazant. Archive of Applied Mechanics **69**, 703 (1999).

[72] L. Sutherland, R. Shenoi, and S. Lewis. Composites Science and Technology **59**, 209 (1999).

[73] D. Montgomery. *Design and Analysis of experiments* (John Wiley & Sons, Singapore, 1994), 3 edition.

[74] W. Connover. *Practical Nonparametric Statistics* (John Wiley & Sons, New York, USA, 1999), 3 edition.

[75] S. Heyden. *A Network Model Applied to Cellulose Fibre Materials*. Licentiate's Thesis, Lund University, Division of Structural Mechanics, Sweden (1996).

[76] S. Heyden. *Network Model for the Evaluation of Mechanical Properties of Cellulose Fibre Fluff* . Ph.D. Thesis, Lund University, Division of Structural Mechanics (2000).

[77] S.-C. Kim, Z.-H. Yoon, and T.-H. Kwon. Physica A p. 320 (1997).

[78] A. Balankin and F. Sandoval. Revista Mexicana de Física **43**, 545 (1997).

[79] J. Schmittbuhl and K. Måløy. Phys. Rev. Lett. **78**, 3888 (1997).

[80] A. Delaplace, J. Schmittbuhl, and K. Måløy. Phys. Rev. E **60**, 1337 (1999).

[81] J. Kertesz, V. Horváth, and F. Weber. Fractals **1**, 67 (1993).

[82] A. Balankin, J. Mendez, G. Mancilla, and G. Urriolagoitia. Int. J Fracture **90**, 57 (1998).

[83] A. Balankin and O. Susarrey. Philosophical Magazine Letters **79**, 629 (1999).

[84] B. Donner. In *The Fundamentals of Papermaking Materials*, edited by C. Baker (Pira International, Leatherhead, United Kingdom, 1997), p. 1215. Transactions of the 11th Fundamental Research Symbosium.

[85] N. Provatas, M. Alava, and T. Ala-Nissilä. Phys. Rev. E **54**, 54 (1996).

[86] J. Weiss, F. Lahaie, and J. Grasso. J. Geophys. Res. **105**, 433 (2000).

[87] C. Maes, A. V. Moffaert, H. Frederix, and H. Strauven. Phys. Rev. B **57**, 4987 (1998).

[88] J. Åström, H. Herrmann, and J. Timonen. European Physical Journal E **4**, 273 (2001).

[89] M. Minossi, G. Caldarelli, L. Pietronero, and S. Zapperi. Private communication (2002). Cond-mat/0207433.

[90] K. Chen, P. Bak, and S. Obukhov. Physical Review A **43**, 625 (1991).

[91] A. Garcimartín, A. Guarino, L. Bellon, and S. Ciliberto. Phys. Rev. Lett. **79**, 3202 (1997).

[92] S. Zapperi, P. Ray, H. Stanley, and A. Vespignani. Phys. Rev. Lett. **78**, 1408 (1997).

[93] A. Tanaka, H. Kettunen, K. Niskanen, and K. Keitaanniemi. J. Pulp Paper Sci. **26**, 385 (2000).

[94] M. Kellomäki. *Rigidity and Transient Wave Dynamics of Random Networks*. Ph.D. Thesis, Jyväskylä University, Department of Physics (1998).

[95] R. Vuohelainen. *A Non-Contacting Method for Measuring Sheet Grammage and Thickness Using Acoustic Pulse Techiniques*. Ph.D. Thesis, Helsinki University, Department of Physics (1998).

[96] M. Johnson, Y. Berthelot, P. Brodeuer, and L. Jacobs. Ultrasonics **34**, 703 (1996).

[97] M. Johnson and Y. Berthelot. J. Acoust. Soc. Am **101**, 2986 (1997).

[98] M. Lysak. Engineering Fracture Mechanics **55**, 443 (1996).

[99] L. Salminen, J. Rosti, J. Pulakka, K. Fallström, M. Alava, and K. Niskanen. to be published (2003).

[100] L. Salminen. *The Measurement and Analysis of Paper Stress-Strain-Curve*. Master's Thesis, Helsinki University of Technology, Department of Technical Physics (1996).